JOURNAL OF CHEMICAL INFORMATION AND MODELING

Article

pubs.acs.org/jcim

Insight into Crizotinib Resistance Mechanisms Caused by Three Mutations in ALK Tyrosine Kinase using Free Energy Calculation Approaches

Huiyong Sun,[†] Youyong Li,*[,†] Dan Li,[‡] and Tingjun Hou*[,†,‡]

[†]Institute of Functional Nano & Soft Materials (FUNSOM) and Jiangsu Key Laboratory for Carbon-Based Functional Materials & Devices, Soochow University, Suzhou, Jiangsu 215123, China

[‡]College of Pharmaceutical Sciences, Zhejiang University, Hangzhou, Zhejiang 310058, China

Supporting Information

ABSTRACT: As a safe and efficacious drug, crizotinib was approved by the U.S. Food and Drug Administration (FDA) in 2011 for the treatment of advanced fusion-type nonsmall-cell lung cancer. Although high response ratio was detected from the patients treated with crizotinib, the cancer has eventually conferred resistance to crizotinib. Several drug resistance mutations have been found in the anaplastic lymphoma kinase (ALK) tyrosine kinase domain as the target for crizotinib, but the drug resistance mechanisms remain unclear. Therefore, in this study, the adaptive biasing force (ABF) method and two-end-state free energy calculation approaches were employed to elucidate the resistance mechanisms of crizotinib induced by the mutations L1152R, G1202R, and S1206Y. The ABF simulation results suggest that the reaction coordinates for the unbinding processes of crizotinib from the binding pockets of the mutated ALKs is different from that of the wild type ALK. The potentials of mean force for the crizotinib unbinding and the binding free energies predicted by the two-end-state free energy calculations are consistent with the experimental data. Our results indicate that the three mutations weaken the binding affinity of crizotinib obviously and lead to drug resistance. The free energy decomposition analysis illustrates the importance of the loss of two important H-bonds in the L1152R and S1206Y mutants on drug resistance. The entropy analysis shows that the entropy term plays a critical role in the substantial change of the conformational entropies of G1202R and L1152R. Our results reveal the mechanisms of drug resistance and provide vital clues for the development of new inhibitors to combat drug resistance.

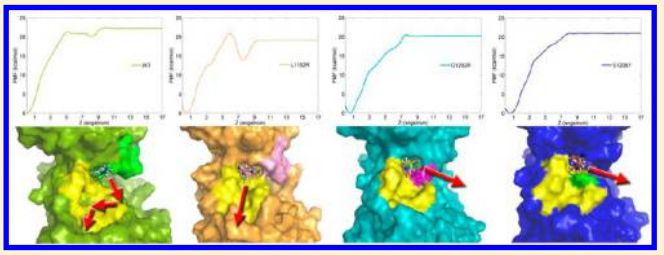

INTRODUCTION

The fusion gene between echinoderm microtubule-associated protein-like 4 (EML4) and anaplastic lymphoma kinase (ALK) is found in 3−7% of nonsmall-cell lung cancer (NSCLC) patients,[1−5] which constitute approximately 8000 new cases in America and 40 000 cases worldwide per year.[6] In 2007, ALK was identified as a potential drug target,[7] and after only 4 years, crizotinib, an oral small-molecule inhibitor of ALK,[8] was approved by the U.S. Food and Drug Administration (FDA) for the treatment of advanced NSCLC containing ALK rearrangements. The high response ratio (55−72%)[9] made crizotinib one of the most successful drugs in the cancer war.[10]

However, cancers eventually confer resistance to their drugs. The same doom has happened to the ALK tyrosine kinase domain. Several *in vivo* resistance mutations in ALK, including L1196M, C1156Y,[11] F1174L,[12] L1152R,[13] G1269A,[14] G1202R, S1206Y, and an insert mutation 1151Tins,[15] have been detected recently. As shown in Figure 1, L1196 M and G1269A both locate at the ATP-binding pocket of ALK, and it is believed that the resistance mechanism of these two mutations is similar to that of T790 M in epidermal growth factor receptor (EGFR) in NSCLC to gefitinib,[16] as the mutations L1196 M and G1269A may directly hinder the binding of crizotinib to the ALK domain due to the substitution of a small amino acid by a larger one.[9,11,14,17,18] Although the drug resistance mutation F1174L may not affect the binding of crizotinib directly, Bresler et al. showed that it can enhance the affinity of ATP for the mutated ALK,[19] and Berry et al. proved that F1174L reduces the turnover of MYCN protein and thus stabilizes the protein, which enhances the downstream signal transduction.[20] The insertion mutation 1151Tins may disrupt a critical H-bond between T1151 and the carbonyl of E1129 backbone, thus leading to changes in the affinity of ATP for ALK.[15,18] The resistance mutations G1202R and S1206Y locate at the solvent front, and it is likely that the bulky residues diminish the affinity of crizotinib for ALK.[15] Although the mutations L1152R and C1156Y locate a bit distant from the crizotinib-binding pocket (approximately 12 and 15 Å from the binding site, respectively), they both confer resistance to crizotinib. Sasaki et al. believed that the mutation L1152R may not only reduce the binding affinity of crizotinib but also modify the activity of the ALK tyrosine kinase, making it more easily

Received: March 28, 2013
Published: August 18, 2013

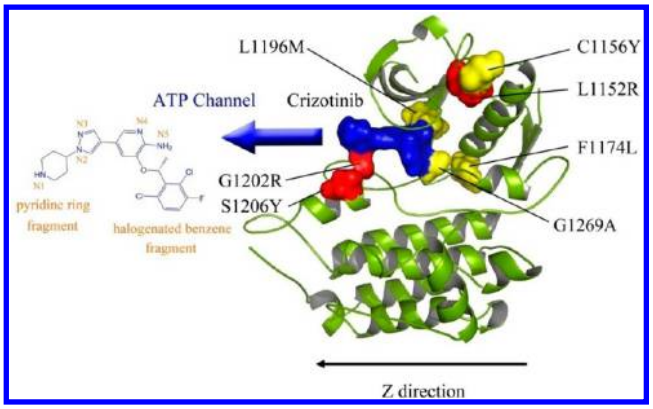

Figure 1. Representation of the ALK tyrosine kinase (green) with several mutations (red and yellow) and crizotinib (3D-surface model and 2D-structure model in blue). The three studied mutations, including L1152R, G1202R, and S1206Y, are colored in red. The direction of the ATP channel along the *Z*-axis is labeled in blue.

been activated.[13] Recently, Shen et al. observed that the mutation C1156Y triggers a conformational change of the P-loop (loop 1122−1130), β-sheet 1145−1152, and α-C helix (α-helix 1157−1174), which thus forces crizotinib to move to a new position to keep balance and therefore reduces the affinity of crizotinib for ALK.[21,22]

Although most of the drug resistance mutations have been studied, the resistance mechanisms for several of them remain ambiguous, such as L1152R, G1202R, and S1206Y. Therefore, in this study, by employing adaptive biasing force (ABF) simulations, molecular dynamics (MD) simulations, and free energy calculations, we mapped the reaction coordinates (RCs) of the unbinding of crizotinib from the binding pockets of the three mutated ALKs (L1152R, G1202R, and S1206Y) and the wild-type (WT) ALK, predicted the binding affinities of crizotinib with the mutated and WT ALKs, and then proposed the drug resistance mechanisms for the studied mutations. The ABF results show the that RCs of crizotinib for the three mutated ALKs are different from that for the WT ALK. On the basis of the conventional MD simulations, the affinities of crizotinib with the WT and three mutated ALKs were predicted by the molecular mechanics/generalized born surface area (MM/GBSA) methodology, and the predicted binding free energies are in reasonable agreement with the experimental data. The gas phase enthalpy and entropy terms are essential for the reduced affinities of crizotinib caused by the resistance mutations. The flexibility of the P-loop (loop 1122−1130) and loop 1264−1259 plays a vital role in the difference of the entropies between the bound and unbound states of ALKs.

MATERIALS AND METHODS

Preparation of the Starting Systems. The X-ray crystallographic structures of ALK complexed with crizotinib (PDB entry 2XP2; resolution 1.9 Å[23]) and free ALK (PDB entry 3L9P; resolution 1.8 Å[24]) were used as the initial structures. The missing residues of the structures, such as H1124−G1125, G1137−S1143, P1218−S1219, S1281−A1289, and the terminal residue Y1401 in the free ALK, were modeled using the loop module in the SYBYL-X1.2 package.[20] The residue L1152, G1202 or S1206, was mutated to R, R, or Y with the Biopolymer module in SYBYL-X1.2, followed by a position adjustment to minimize the influence of the newly added side chain on the surroundings.

Crizotinib was optimized by the Hartree−Fock method with the 6-31G* basis set, and then, the electrostatic potentials were calculated by using the Gaussian 03 program.[25] The atomic partial charges of crizotinib were obtained by using the RESP fitting method[26] implemented in Ambertools.[27] The general Amber force field (gaff)[28] and Amber99SB force field[29] were used for crizotinib and proteins, respectively. Counterions were added to neutralize the charge of the system, and each ALK system (bound-state and unbound-state ALKs) and crizotinib-free system were then immersed in TIP3P[30] water boxes with 8 and 40 Å out of the solute atoms in each direction, respectively.

Conventional MD Simulations. The NAMD 2.8 simulation package[31] was employed for both the conventional MD and ABF simulations. The particle mesh Ewald (PME)[32] algorithm was employed for the long-range electrostatics in both minimization and MD simulation stages. A five-step minimization protocol was used to optimize the systems: (1) All heavy atoms were restrained with 5 kcal/mol·Å^2, and only hydrogen atoms were allowed to move (5000 steps). (2) The water molecules and ions were also permitted to move (5000 steps). (3) The side chains of proteins were relaxed (5000 steps). (4) Crizotinib and the backbone atoms within 5 Å of the mutation site in each mutated ALK were optimized (5000 steps), and (5) the whole system was minimized for 20 000 steps.

In the MD simulation phase, a 10 Å cutoff was used to handle short-range interactions. All covalent bonds involving hydrogen atoms were constrained with the SHAKE algorithm.[33] Each system was gradually heated from 0 to 310 K within 1.2 ns with the backbone of proteins restrained (5 kcal/mol·Å^2) in the *NVT* ensemble, and then, the restraint was gradually relaxed within 0.2 ns from 5 to 0 kcal/mol·Å^2 in the *NPT* ensemble with the target pressure of 1 atm and the target temperature of 310 K. The Poisson Piston algorithm was used to control the pressure.[34] After that, more than 13.5 ns equilibrating calculations were preformed to produce trajectories. The time step was set to 2 fs, and the atom coordinates were collected at the interval of 5 ps (200 frames/ns).

Adaptive Biasing Force Simulations. ABF[35,36] has shown efficiency in free energy calculation based on a given reaction coordinate.[37−39] Because the added biasing can cancel the local barriers, and as a result, all values of the reaction coordinate are sampled with equal probability and the biased molecule can go with a free-diffusion-like behavior along the reaction coordinate that can markedly improve the accuracy of free energy calculation. More importantly, it may represent a reversible process along the reaction coordinate when full sampling is achieved. Therefore, in this study, the ABF method was employed to study the change of free energy of crizotinib moving out of the binding pocket along the RC (*Z*-axis). As the mutation may affect the binding mode of crizotinib, the average structures from the conventional MD trajectories were used as the initial structures for the ABF simulations. The ATP channel in kinase usually acts as the gateway for the binding/unbinding of drugs or substrates,[40] and thus, by using Caver 2.0 module in PYMOL,[41] the direction of the largest pocket along the ATP channel (Figure 2) was set as the direction of the RC (Figure 1), which was determined by the distance between C_α of Leu77 and N_2 of crizotinib (parallel to the ATP channel direction, not shown in the figure). The direction of the RC was then rotated to the *Z*-axis, and a rectangle water box that is 30 Å out of the solute in the +*Z* direction was added for the ABF simulations.

In the minimization phase, only the water molecules and ions were allowed to move. After the minimization, 1 ns MD

dx.doi.org/10.1021/ci400188q | J. Chem. Inf. Model. 2013, 53, 2376−2389

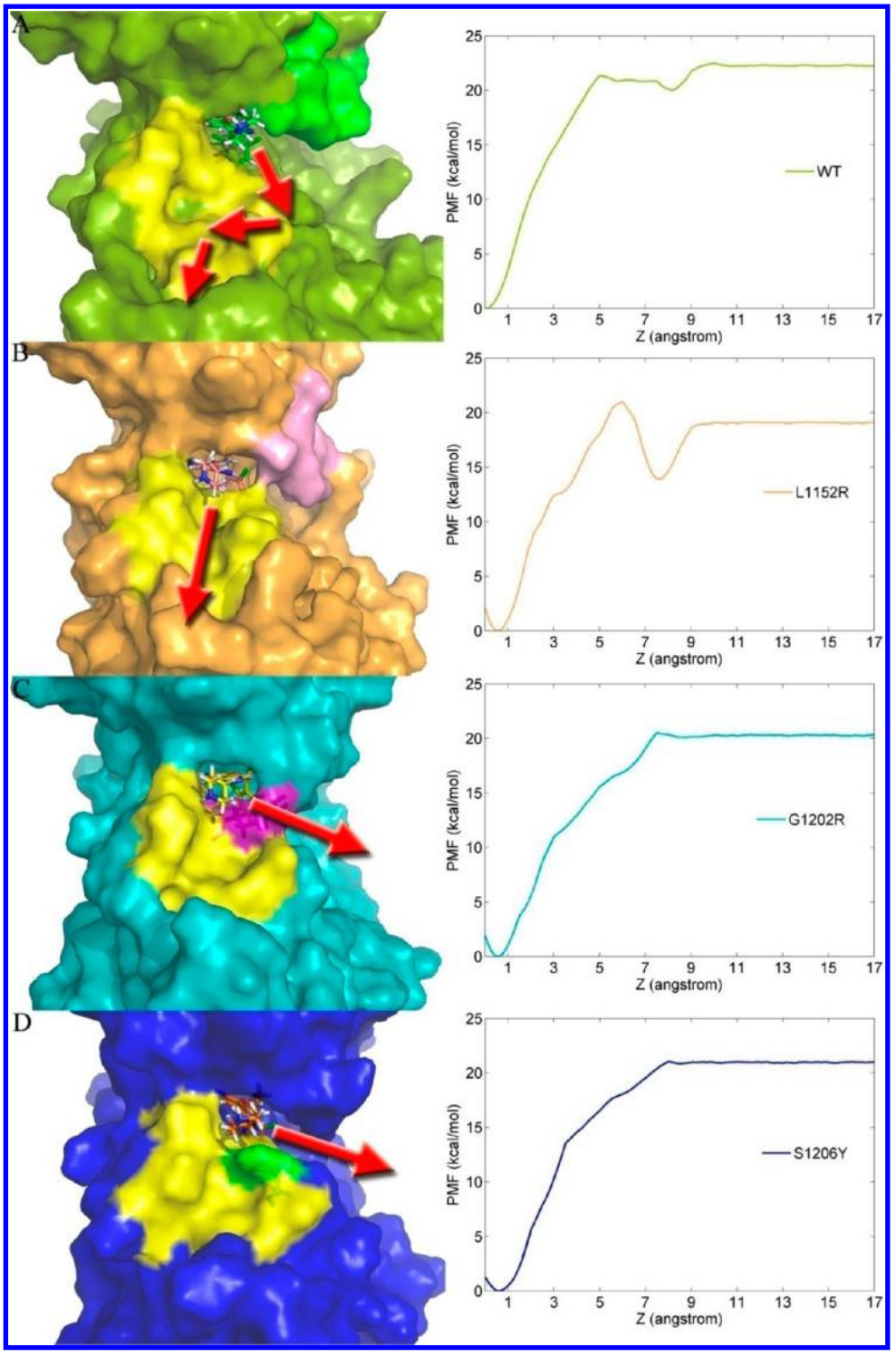

Figure 2. Initial structures and the PMFs of the WT (green) and three mutated ALKs (orange in L1152R, cyan in G1202R, and blue in S1206Y). The direction of the crizotinib unbinding from the binding pocket is labeled in red arrows with a Z-like route in WT and the straight-like routes in L1152R, G1202R, and S1206Y, though different directions are chosen.

simulations were preformed in NTP ensemble to equilibrate the water molecules and ions with the solutes still constrained. In the phase of the ABF simulations, the residues out of 12 Å of crizotinib were restrained with 5 kcal/mol·Å^2 to guarantee the direction of the RC. All the RCs were separated into 34 windows with 0.5 Å/window and 0.01 Å/bin (50 bin/window). Upper and lower wall constants were both set to 50 kcal/mol·Å^2 in high barrier regions and 10 kcal/mol·Å^2 in low barrier regions to ensure full sampling. The *fullSamples* parameter was set to 1000 at each window prior to biasing. Respetively, 6 and 3 ns MD simulations were performed for the windows involved in large and low barrier regions, which guaranteed the convergence of the potential of mean force (PMF) as shown in Supporting Information Figure S1. A total of ∼680 ns MD simulations were performed for the four systems (∼170 ns for each system).

dx.doi.org/10.1021/ci400188q | *J. Chem. Inf. Model.* 2013, 53, 2376−2389

The PMF was finally cumulated from the biasing force along the Z-axis.

Due to the controversy of the difference between the standard binding free energy (ΔG°) and the PMF depth (ΔW_{PMF}, $W_{\mathrm{PMF\text{-}lowest}} - W_{\mathrm{PMF\text{-}highest}}$) derived directly from the biased MD simulations,[42−45] the Henchman's method was employed to calculate the standard binding free energy[42] to give a comparison. The standard binding free energy can be calculated as follows (detailed information can be found in ref 42):

$$\Delta G^\circ = \Delta W_{\mathrm{PMF}} - RT \ln\left(\frac{L_b A_u}{V^\circ}\right) \quad (1)$$

$$L_b = \int_{\mathrm{bound}} \exp\left(\frac{-W_{\mathrm{PMF}}(z)}{RT}\right) \mathrm{d}z \quad (2)$$

ΔG° represents the standard binding free energy, and it can be decomposed into two components: the energy change between the bound and unbound sections of the PMF (ΔW_{PMF}), which can be directly extracted from the ABF simulations, and a volume-associated term, where V° is the standard-state volume (V° = 1661 Å^3) and L_b is a bound-state-associated length, which is the configurational integral of the PMF from the lowest region (bound-state, the lowest region is set to 0 kcal/mol) to the highest region (unbound-state), and A_u is the cross-sectional area detected by the unbound-state ligand, which, in fact, is the cross-sectional area of the period water box (cell) of the system because the unconstrained framework was used in the ABF simulations.

MM/GBSA Free Energy Calculations and Residue Decomposition. The MM/GBSA method has been widely employed to study drug resistance caused by energy loss.[46−49] Although free energy perturbation (FEP) and thermodynamic integration (TI) methods are more theoretically rigorous,[50−53] MM/GBSA also shows the obvious advantage that it can be accurately decomposed into several terms, including van der Waals, electrostatics, polar part of desolvation, nonpolar part of desolvation, and entropy contribution, and this brings convenience to investigate which energy term(s) was influenced by drug resistance mutation. In MM/GBSA, the binding free energy can be calculated as follows:[54−56]

$$\Delta G_{\mathrm{bind}} = G_{\mathrm{com}} - (G_{\mathrm{rec}} + G_{\mathrm{lig}}) \quad (3)$$

$$\Delta G_{\mathrm{bind}} = \Delta H - T\Delta S \approx \Delta E_{\mathrm{MM}} + \Delta G_{\mathrm{sol}} - T\Delta S \quad (4)$$

$$\Delta E_{\mathrm{MM}} = \Delta E_{\mathrm{internal}} + \Delta E_{\mathrm{electrostatic}} + \Delta E_{\mathrm{vdW}} \quad (5)$$

$$\Delta G_{\mathrm{sol}} = \Delta G_{\mathrm{GB}} + \Delta G_{\mathrm{SA}} \quad (6)$$

$$\Delta G_{\mathrm{SA}} = \gamma \Delta A + b \quad (7)$$

where ΔG_{bind} denotes the binding free energy between ligand and receptor, and it can be decomposed into three terms: molecular mechanical energy term (ΔE_{MM}), solvation energy term (ΔG_{sol}), and entropy term ($-T\Delta S$). Moreover, the change of molecular mechanical energy is noted as the change of gas phase enthalpy, which consists of the change of internal energy ($\Delta E_{\mathrm{internal}}$), that of electrostatic energy (ΔE_{ele}), and that of van der Waals energy (ΔE_{vdW}). By using a single trajectory strategy, $\Delta E_{\mathrm{internal}}$ is canceled between ligand, receptor, and complex, which can significantly reduce the noise in most cases,[47] but it may lose the energy associated with conformational change when a free ligand binds to a free receptor. The change of solvation energy (ΔG_{sol}) contains the polar part (ΔG_{GB}) and the nonpolar part of the desolvation energy (ΔG_{SA}).

In this study, the GB model ($\mathrm{GB}^{\mathrm{OBC1}}$) with the parameters developed by Onufriev and co-workers[57] was chosen for the polar desolvation energy calculation because it gave the best ranking results compared with several other GB models according to our previous study.[58,59] The interior dielectric constant was set to 1, and the outer dielectric constant, to 80. Here, the modified bondi2 atomic radii[57] were employed for the polar solvation energy calculation, since it was recommended to be compatible with the $\mathrm{GB}^{\mathrm{OBC1}}$ model in Amber. The nonpolar part of desolvation (ΔG_{SA}) was calculated by eq 7, where ΔA represents the change of the solvent accessible surface area (SASA) of the system calculated by the LCPO algorithm,[60] and the fitting coefficients γ and b were set to 0.0072 kcal/mol·Å^2 and 0, respectively. The last term $-T\Delta S$ of eq 4 is the conformational entropy difference between the bound and unbound state of system.[61] Here, normal-mode analysis (NMA) was used for the calculation of the conformational entropy, and as the high computational demand, only 40 snapshots extracted from the last 10 ns of the conventional MD trajectories were used. The distance-dependent dielectric of $4r_{ij}$ was used to mimic the solvent dielectric change from the solute to solvent, where r_{ij} is the distance between two atoms i and j. Both single MD trajectory and separated MD trajectory strategies were used in free energy calculation due to the controversy above, and all the MM/GBSA free energy calculations were performed by using the *MMPBSA.py* module in Ambertools 1.5.[62]

The nonbonded interactions play a critical role in the binding of ligands and receptors,[63,64] and these can indeed be affected by mutations.[21,65] Therefore, only the nonbonded interactions (ΔE_{vdw} and ΔE_{ele}) were decomposed into residue−ligand pairs from the last 10 ns MD trajectories. All the parameters were derived from the MD simulation protocol, and the calculation was performed by NAMD 2.8.[31]

Principal Component Analysis (PCA). PCA or essential dynamics simulation has been proved to be efficient in exploring the motions of proteins.[21,66−68] Here, the positions of the C_α atoms in proteins were used to calculate the fluctuant covariance of residues according to the following equation:

$$c_{ij} = \langle \Delta r_i \cdot \Delta r_j \rangle \quad (8)$$

where c_{ij} is the fluctuant covariance of two C_α atoms i and j, Δr is the distance between the current position and the average position of an atom, and $\langle\rangle$ denotes the average over the 13.5 ns MD trajectories. The first eigenvector which, in most cases,[67,68] can take about 20% of the total motion of proteins, was used to project the main direction of the motion of proteins.

Conformational Entropy Analysis. Considering that the conformational entropy is positively correlated with the fluctuation of atoms,[69] we calculated the average fluctuant covariance of the heavy atoms of the residues within 12 Å of crizotinib based on the last 10 ns MD trajectories of the bound-state and unbound-state ALKs using eq 8.

Video Preparation. Videos were prepared for the intuitive observation of the unbinding processes of crizotinib from the binding pockets. Twenty-three second videos were produced for WT (Supporting Information Video S1) and L1152R (Supporting Information Video S2), and 20 s videos were prepared for G1202R (Supporting Information Video S3) and S1206Y (Supporting Information Video S4). The videos broadcast with the reaction coordinate by 0.5 Å/s, and thus these videos denote 0−11.5 Å of the RCs for WT and L1152R, and 0−10 Å of the RCs for G1202R and S1206Y.

dx.doi.org/10.1021/ci400188q | J. Chem. Inf. Model. 2013, 53, 2376−2389

Table 1. Binding Free Energies of Crizotinib Complexed with the WT and Three Mutated ALKs Using Various Protocols (kcal/mol)

name	WT	L1152R	G1202R	S1206Y
ΔW_{PMF}[a]	−22.27 ± 0.04	−19.09 ± 0.03	−20.29 ± 0.03	−20.96 ± 0.03
ΔG°[b]	−22.40 ± 0.04	−19.29 ± 0.03	−20.43 ± 0.03	−21.27 ± 0.03
$\Delta G_{bind\text{-}single}$[c]	−24.95 ± 0.02[e]	−17.33 ± 0.40	−22.33 ± 0.21	−22.68 ± 0.19
$\Delta G_{bind\text{-}separate}$[d]	−67.32 ± 4.71	−0.04 ± 4.75	−13.42 ± 4.61	−21.86 ± 4.78
IC_{50} (nM)	64[f]/26.5[g]	853[f]	242.4[g]	120.8[g]
Fold change	1	12.5[f]	9[g]	5[g]
ΔG_{exp}	~13[h]			

[a]Potential of mean force depth based on 11−17 Å of the reaction coordinate. [b]Standard binding free energy calculated using Henchma's method.[42] [c]Binding free energy calculated using single MD trajectory protocol. [d]Binding free energy calculated using separated MD trajectory protocol. [e]Standard deviations based on two blocks (block 1 6−10 ns, block 2 11−15 ns). [f]IC_{50} values derived from ref 13 using the Ba/F3 cell line. [g]IC_{50} values derived from ref 15 using the Ba/F3 cell line. [h]Experimental binding free energy estimated by $\Delta G_{exp} = -RT \ln(1/K_i)$ from ref 17 (310 K) using the Ba/F3 cell line.

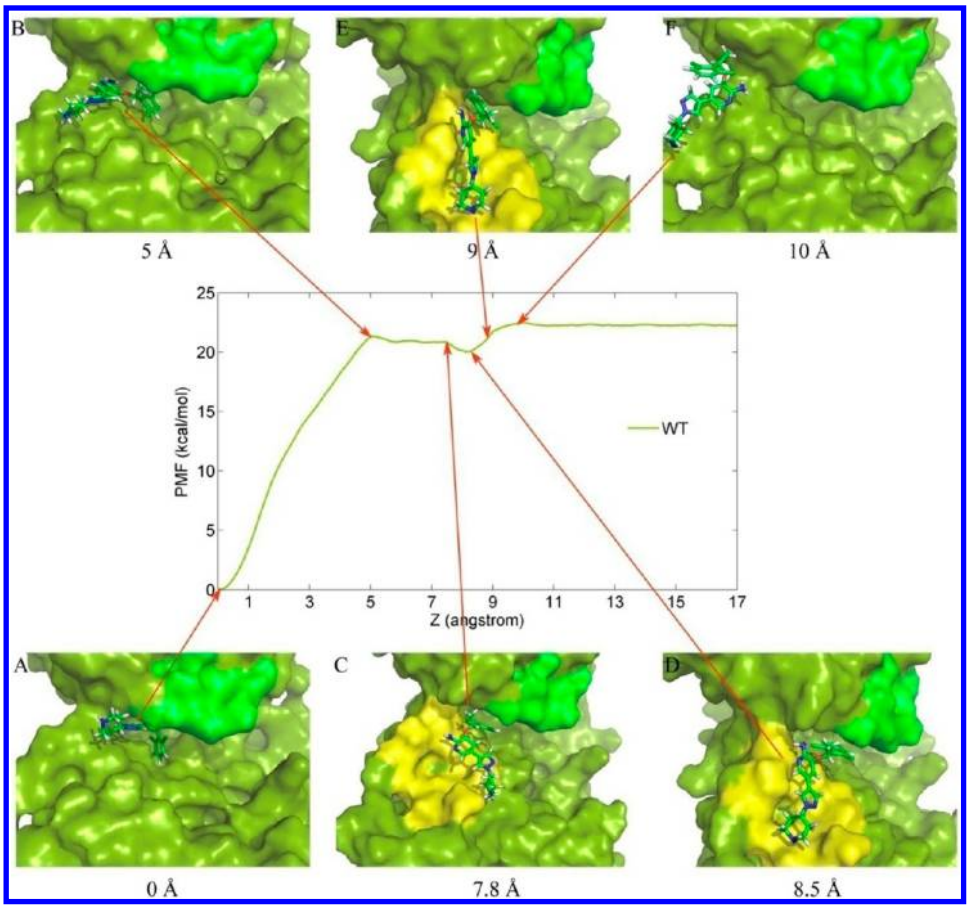

Figure 3. Conformation of crizotinib along the *Z*-axis in the WT ALK. The yellow region (C−E) denotes the necessary binding channel for crizotinib moving out of (or into) the binding pocket, and the green region (A−F) represents the important loop (loop 1122−1130 or P-loop) for the binding of crizotinib.

RESULTS AND DISCUSSION

Potential of Mean Force (PMF) along the Reaction Coordinate (RC). Because the mutation may affect the conformation of the residues around the mutation site,[21] it is necessary to get an equilibrium conformation for postanalysis. Therefore, we performed 15 ns conventional MD simulations for each system to generate the equilibrium structure for the ABF simulations. As shown in Figure S2 in the Supporting Information, all the MD simulations are stable over the 15 ns trajectories, with the root-mean-square deviations (RMSD) less than 2 Å of the protein backbones and the heavy atoms in crizotinib (Figures S2A−D), and the root-mean-square fluctuations (RMSF) less than 2.5 Å in most regions, if not considering the very flexible loops in 1137−1144, 1213−1222, and 1280−1292 (Figure S2E). Thus, the average structures from the conventional MD simulations are satisfactory to be used as the initial structures for the ABF simulations.

As shown in Figure 1, the direction of the largest pocket of the ATP channel was chosen as the reaction coordinate, and it was rotated along the *Z*-axis for the projection of the biasing force. Figure 2 shows the initial structures of the WT (dark green, A) and three mutated ALKs (orange for L1152R, B; cyan for G1202R, C; blue for S1206Y, D), and their corresponding PMFs

dx.doi.org/10.1021/ci400188q | J. Chem. Inf. Model. 2013, 53, 2376−2389

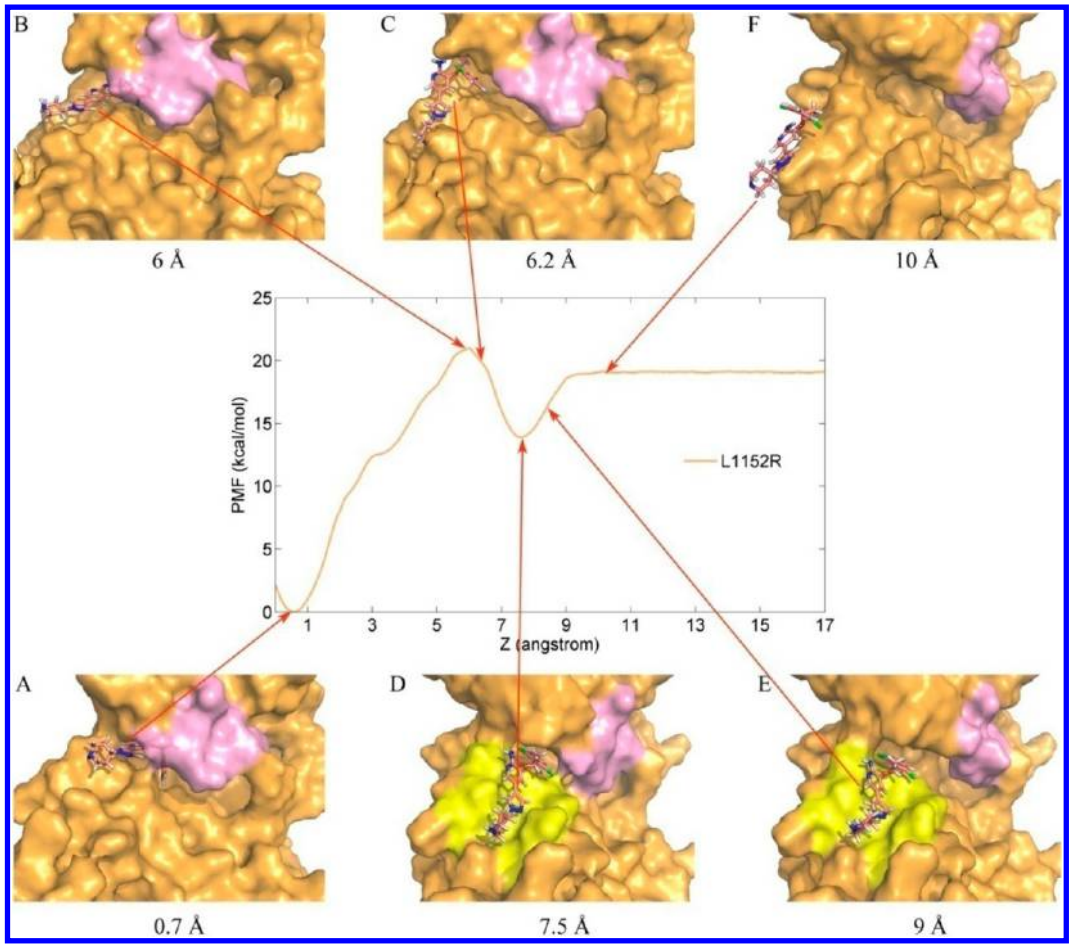

Figure 4. Conformation of crizotinib along the *Z*-axis in the mutated ALK L1152R. The yellow region (D and E) denotes the necessary binding channel for crizotinib moving out of (or into) the binding pocket, and the pink region (A–F) represents the important loop (loop 1122–1130 or P-loop) for the binding of crizotinib. The P-loop may be located too low to hinder the crizotinib out of (or into) the binding site, and thus, a large barrier is formed when crizotinib gets out of the binding pocket (B and C).

for the crizotinib unbinding cumulated from the ABF simulations. It is obvious that the PMF curves for the three mutated ALKs are different from that for the WT ALK. There is a large barrier (>7 kcal/mol) at ∼6 Å of the RC for L1152R while no apparent barrier for G1202R and S1206Y, and a small barrier (∼1 kcal/mol) crosses 5–8 Å for WT. Moreover, no rising of the PMFs was observed at ∼9 Å of the RCs for G1202R and S1206Y, whereas a rising of the PMFs more than 2.5 kcal/mol and approximately 5 kcal/mol was observed at ∼9 Å for WT and L1152R, respectively. The superimposition of the 4 PMFs is shown in Supporting Information Figure S3. For convenience, only the minimum positions of energy were overlapped with the PMF value labeled with 0 kcal/mol. Thus, the higher the curve, the more energy is released during the drug binding to their targets. It is apparent that the PMF curve for WT (green) is the highest among the four systems with the decrease of the PMF close to 2 kcal/mol for G1202R and more than 3 and 1 kcal/mol for L1152R and S1206Y, respectively (the corresponding PMF depth, ΔW_{PMF}, can be found in Table 1). That is to say, crizotinib forms the strongest affinity with the WT ALK, and the three mutations are able to cause resistance to crizotinib.

The processes of the crizotinib unbinding from the WT and three mutated ALKs (L1152R, G1202R, and S1206Y) are illustrated in Figures 3, 4, 6, and 7. As shown in Figure 3, crizotinib gradually moves from the binding pocket with the increase of the biasing potential added to crizotinib. At ∼5 Å of the RC, the biasing potential reaches the first maximum value where the drug is approximately flattened at the entrance of the pocket with half of the molecule out of the pocket (Figure 3B). When the molecule moves out of the pocket, the backbone of the drug rotates to the P-loop side (∼7.8 Å of the RC), because there is a larger space for crizotinib moving out without barriers (Figure 3C and Supporting Information Video S1 (14 s)). After the nearly flat region of the PMF (5.0–8.0 Å of the RC), crizotinib moves (rotates) to a new balanced position (∼8.5 Å of the RC), as illustrated in Figure 3D. The drug adsorbs at the yellow region that is possibly a binding channel (∼8.5 Å of the RC) for inhibitors getting into (or out of) the pocket, and a large biasing force (equal to a PMF of 2.5 kcal/mol at 9–10 Å of the RC) is needed to pull the drug away from the channel to the second maximum (∼10 Å) (Figure 3F and Supporting Information Video S1). As a result, a *Z*-like route was employed by crizotinib in WT to move out of the binding pocket as shown in Figure 2A.

Similar behavior was observed for L1152R (Figure 4D, Supporting Information Video S2). The drug also absorbs at the binding channel (yellow area at ∼7.5 Å of the RC), and a much larger biasing force (equal to a PMF of 5 kcal/mol) is needed to pull the drug out of the channel in WT (Figure 4F). However, a big difference was observed at the region 5–7 Å of the RC with a large barrier for L1152R, and the global maximum (∼21 kcal/mol) exists at ∼6 Å of the RC, where the drug is almost out of the

dx.doi.org/10.1021/ci400188q | *J. Chem. Inf. Model.* 2013, 53, 2376–2389

binding pocket (Figure 4B). It is followed by the remarkable decrease of the PMF until it reaches the local minimum at ∼7.5 Å of the RC, where the binding channel is as mentioned above.

It can be seen in Figure 4C and Supporting Information Video S2 (∼12 s) that crizotinib is likely to be "catapulted out" of the pocket, which is different from WT (Figure 3C and Supporting Information Video S1 (∼14 s)). In WT, the direction of crizotinib was rotated to the P-loop side for moving out of the pocket smoothly as mentioned above. Thus, a straight-like, however barrier-existing, route was used by crizotinib in L1152R to move out of the binding pocket (Figure 2B). As shown in Figure 2A and B, the initial (or average) structures of WT and L1152R are different significantly. The P-loop (loop 1122−1130) in L1152R (pink) moves down compared with that in WT (green). Hence, it appears that the P-loop in L1152R may narrow the entrance of the binding pocket. A detailed structure analysis shows that the mutated positively charged residue R1152 (pink) is stable because it forms strong electrostatic interactions with two negatively charged residues D1160 and D1163 (Figure 9A1). However, the bulky side chain of R1152 seriously disturbs the surrounding residues, as illustrated in Figure 9A4. The side chain of R1152 (pink) forces F1127 (pink) to move down from its original position in WT (green) to weaken the steric hindrance between the two residues. Because F1127 locates at the P-loop region (loop 1122−1130), the repulsion between F1127 and R1152 results in the downward moving of the P-loop. Additionally, an essential dynamics or PCA shows that the motion of the P-loop in L1152R goes down with the direction of the motion along approximately the diagonal of the coordinate system [−3.4, 5.6, −4.9] (Figure 5B), while the direction of the motion of WT is approximately 30° along the *Z*-axis [4.8, −0.8, 7.8] (Figure 5A, here the RC was not rotated to the *Z*-axis). Therefore, the downward moving of the P-loop in L1152R is the main reason for producing the large barrier in the RC. Moreover, the attraction of the binding channel at ∼7.5 Å of the RC (Figure 4D) also contributes to the large barrier because it can pull the drug out of the pocket.

The PMFs of G1202R and S1206Y are quite different from those of WT and L1152R. As mentioned above, no rising of the PMFs around 9 Å of the RCs. As illustrated in Figures 6 and 7, before moving out of the pocket, the behaviors of crizotinib are quite similar for WT and L1152R, though the maximum positions of the PMFs are a bit backward for G1202R (∼7.5 Å) and S1206Y (∼8.0 Å) compared with the first maximum positions of the PMFs for WT (∼5 Å) and L1152R (∼6 Å) (Supporting Information Figure S3). Why there is no rising of the PMFs around 9 Å of the RCs for G1202R and S1206Y? It is possible that the mutations hinder the drug diffusing into the binding channel. As shown in Figures 6C and 7C, the mutations (purple area in G1202R and green area in S1206Y) both locate above the binding channel, and hence, it is impossible for the drug to bind to the channel area (yellow area, see Supporting Information Video S3 and S4). Therefore, after moving out of the pocket, the drugs can only go into the surrounding solvent (Figures 6D and 7D) with a straight-like route as that in L1152R, however, in different directions (see Figure 2C and D).

Comparison of Free Energies Calculated by Various Strategies. For each system, the standard binding free energy (ΔG°) and compared with the PMF depth (ΔW_{PMF})[42−45] (detailed information can be found in Supporting Information Table S1). As listed in Table 1, the drugs in the three mutated ALKs show a decrease of the binding free energy with respect to WT. The binding free energies based on the PMF depth

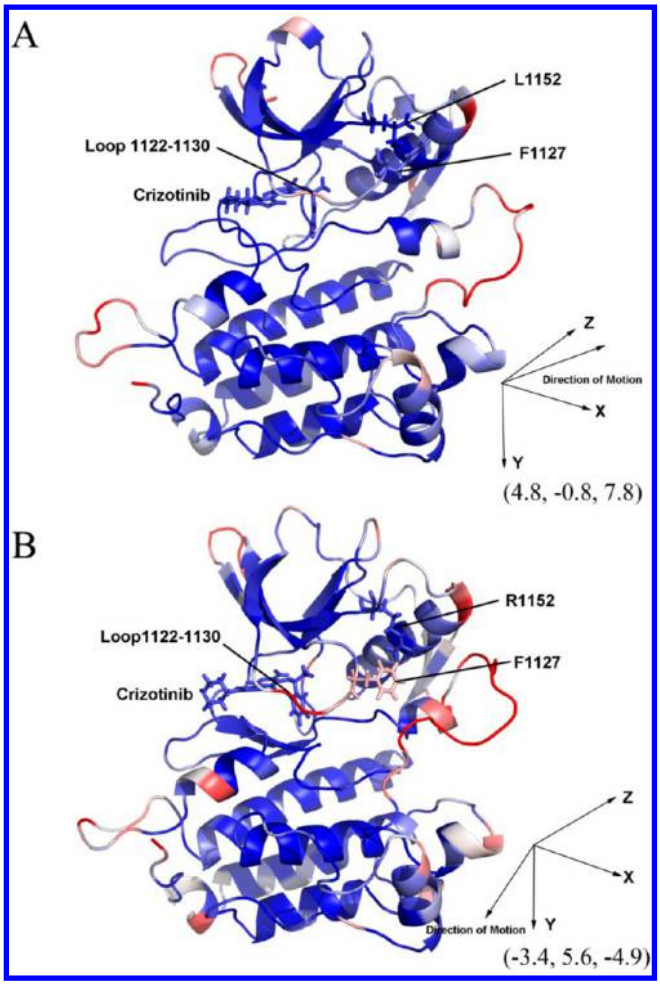

Figure 5. Cartoon models of the motion projections along the first eigenvector for (A) the WT ALK complex and (B) the L1152R ALK complex. The arrows indicate the main direction of the motion, and the amplitude of the backbone motion goes from blue to red. The loop 1122−1130 (P-loop) is involved in a large conformational change in L1152R where the color goes to red compared with that in WT.

(ΔW_{PMF}) and standard binding free energy (ΔG°) are the same with respect to the corresponding systems, that is to say, not much attention should be taken to distinguish the PMF depth and standard binding free energy in our ABF simulation strategy. As the ABF simulations only give the difference of the total free energies along the unbinding pathways, it is hard to give the contributions of each energy term to the energy change between the WT ALK and each mutated ALK. Therefore, based on the trajectories of the conventional MD simulations, we predicted the absolute binding free energies predicted by the MM/GBSA method based on two protocols: single MD trajectory protocol and separated MD trajectory protocol. Compared with the binding free energies calculated by the separated MD trajectories ($\Delta G_{bind\text{-}separate}$, details can be found in Supporting Information Table S2), the binding free energies predicted by single MD trajectory protocol ($\Delta G_{bind\text{-}single}$) give more reasonable results (more close to the experimental value), where the binding free energy $\Delta G_{bind\text{-}single}$ (−24.95 kcal/mol) for WT ALK is much higher than the corresponding binding free energy $\Delta G_{bind\text{-}separate}$ (−67.32 kcal/mol) based on the separated MD trajectories, while the binding free energy $\Delta G_{bind\text{-}single}$ (−17.33 kcal/mol) for L1152R is much lower than that (−0.04 kcal/mol) for the corresponding mutant ALK. Therefore, the analyses will be more

dx.doi.org/10.1021/ci400188q | J. Chem. Inf. Model. 2013, 53, 2376−2389

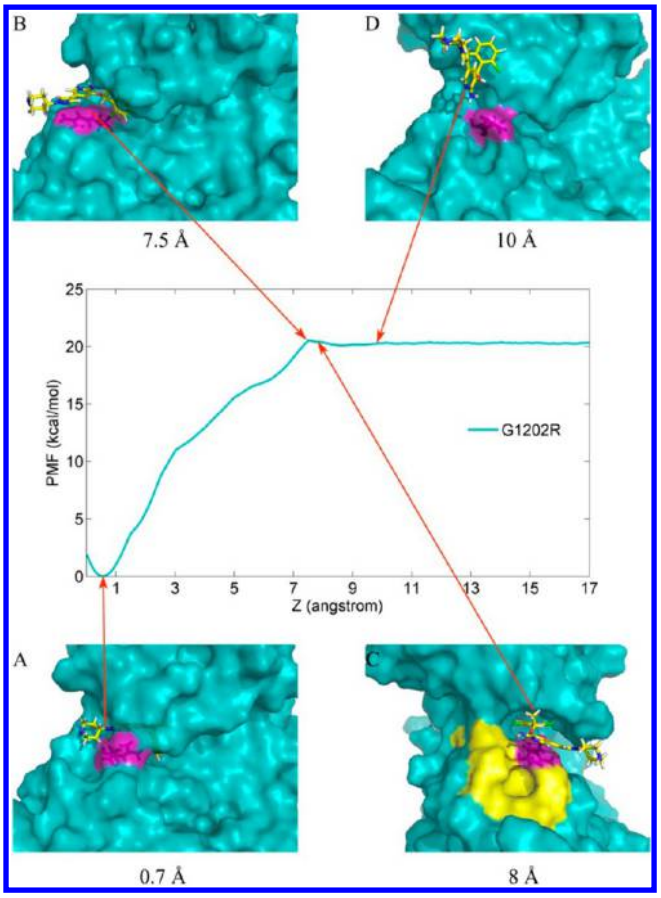

Figure 6. Conformation of crizotinib along the *Z*-axis in the mutated ALK G1202R. The purple area (A–D) represents the mutation site G1202R and the yellow region (C) denotes the necessary binding channel for crizotinib moving out of (or into) the binding pocket.

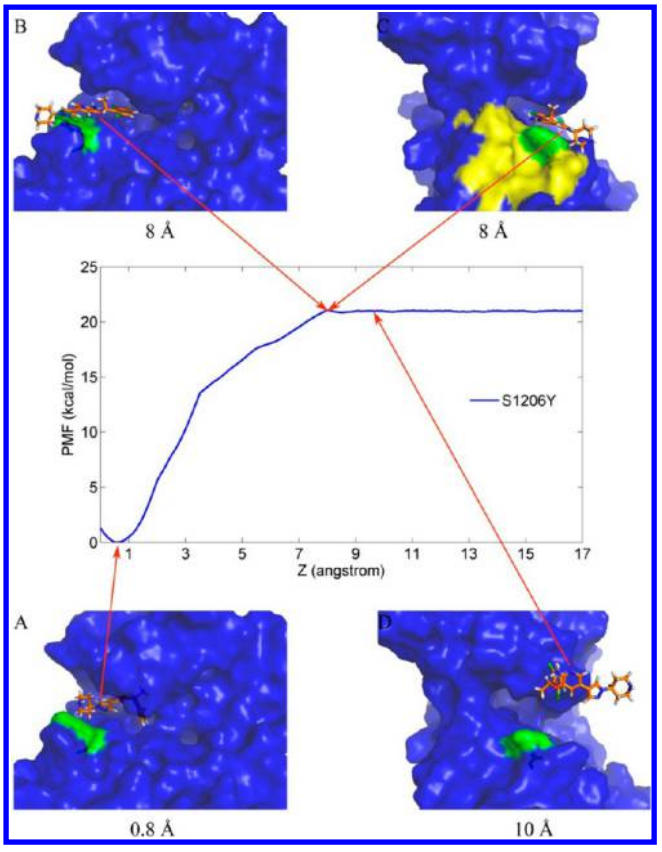

Figure 7. Conformation of crizotinib along the *Z*-axis in the mutated ALK S1206Y. The green region (A–D) represents the mutation site S1206Y, and the yellow region (C) denotes the necessary binding channel for crizotinib moving out (or into) the binding pocket.

focused on the MM/GBSA results based on the single MD trajectories Additionally, it can be found that the ranking of the binding free energies predicted by the four protocols all agree well with the experimental IC_{50}s (fold change), though the absolute values are larger than the experimental binding free energies (Table 1). Since the correct ranking of the binding free energies is usually emphasized in molecular design,[58] it is reasonable to accept the results above.

The analysis of the binding free energies predicted by MM/GBSA based on the single MD trajectories shows that various energy terms contribute differently to the decrease of the binding free energies for the three mutated ALKs (Table 2). Here, we only discussed the nonbonded energy term ($\Delta E_{nonbonded}$) and the entropy term ($-T\Delta S$), due to the fact that the nonbonded energy plays a critical role in the drugs residence time or drug efficiency,[63,64] and the conformational entropy determines the conformational change of the proteins and drugs upon drug binding. As listed in Table 2, the decrease of the nonbonded energy (5.74 kcal/mol) and the increase of the entropy (5.54 kcal/mol) both lead to the decrease of the binding free energy for L1152R. Either the increase of the entropy for G1202R (4.30 kcal/mol) or the decrease of the nonbonded energy for S1206Y (4.20 kcal/mol) causes the total binding free energy declined by 2.62 kcal/mol for G1202R and 2.27 kcal/mol for S1206Y. Therefore, L1152R indeed leads to the most serious drug resistance to crizotinib among the three mutations.

Drug Resistance Mechanisms Characterized by Residue Decomposition and Entropy Analysis. Residue decomposition has been widely used in analyzing drug resistance mechanisms,[21,46−48,70−72] because it can detect the most affected residues and reveal the drug resistance mechanisms in details. Therefore, we used the residue decomposition approach to analyze the resistance mechanisms of the three mutations. As shown in Figure 8A, several residues lost their nonbonded energies to crizotinib in L1152R, including L1122, G1123, D1249, N1254, and D1270. As shown in Table 2 and Supporting Information Figure S4, the decrease of the electrostatic term contributes more to the difference of the nonbonded energies compared with that of the van der Waals term. Further observation shows that two H-bonds in L1152R are impaired, as illustrated in Figure 9A2 and A3 and Supporting Information Figure S7. The H-bond between the fluorine atom in crizotinib and the amide hydrogen in D1270 increases from 2.9 to 3.7 Å in L1152R, while the H-bond between N3 in crizotinib (Figure 1) and the amide hydrogen in G1123 increases from 2.7 to 3.8 Å, caused by the moving out of crizotinib in L1152R (Figure 9A2). Therefore, the loss of the two important H-bonds is the main reason for the reduction of the nonbonded interaction of crizotinib in L1152R. Why crizotinib in L1152R moves more outside of the binding pocket? The electrostatic repulsion of the positively charged mutated residue R1152 forces K1150 to move left (pink), thus hindering crizotinib staying where it is in WT (green, Figure 9A2).

As shown in Figure 9B2, crizotinib in G1202R (yellow) is also more outside than that in WT (green). However, no decrease of

dx.doi.org/10.1021/ci400188q | J. Chem. Inf. Model. 2013, 53, 2376−2389

Table 2. Binding Free Energies of Crizotinib Complexed with the WT and Three Mutated ALKs Using the Single MD Trajectory MM/GBSA Approach (kcal/mol)

name	WT	L1152R	G1202R	S1206Y
ΔE_{vdW}[a]	−49.24 ± 0.02[i]	−48.02 ± 0.50	−51.61 ± 0.33	−48.01 ± 0.15
ΔE_{elec}[b]	−19.66 ± 0.30	−15.12 ± 1.08	−18.67 ± 0.54	−16.68 ± 1.15
ΔG_{GB}[c]	34.70 ± 0.34	31.03 ± 0.94	34.79 ± 0.69	32.63 ± 1.24
ΔG_{SA}[d]	−5.55 ± 0.02	−5.46 ± 0.00	−5.84 ± 0.03	−5.43 ± 0.03
$T\Delta S$[e]	−14.80 ± 0.79	−20.25 ± 1.38	−19.01 ± 0.99	−14.80 ± 0.17
$\Delta E_{nonbonded}$[f]	−68.89 ± 0.16	−63.15 ± 0.27	−70.29 ± 0.44	−64.69 ± 0.16
$\Delta E_{enthalpy}$[g]	−39.75 ± 0.02	−37.58 ± 0.40	−41.34 ± 0.21	−37.48 ± 0.19
ΔG_{bind}[h]	−24.95 ± 0.02	−17.33 ± 0.40	−22.33 ± 0.21	−22.68 ± 0.19

[a]van der Waals energy. [b]Electrostatic energy. [c]Electrostatic contribution to solvation. [d]Nonpolar contribution to solvation. [e]Entropic contribution. [f]Nonbonded energy. [g]Binding free energy in the absence of entropic contribution. [h]Binding free energy. [i]Standard deviations based on two blocks (block 1 6−10 ns, block 2 11−15 ns).

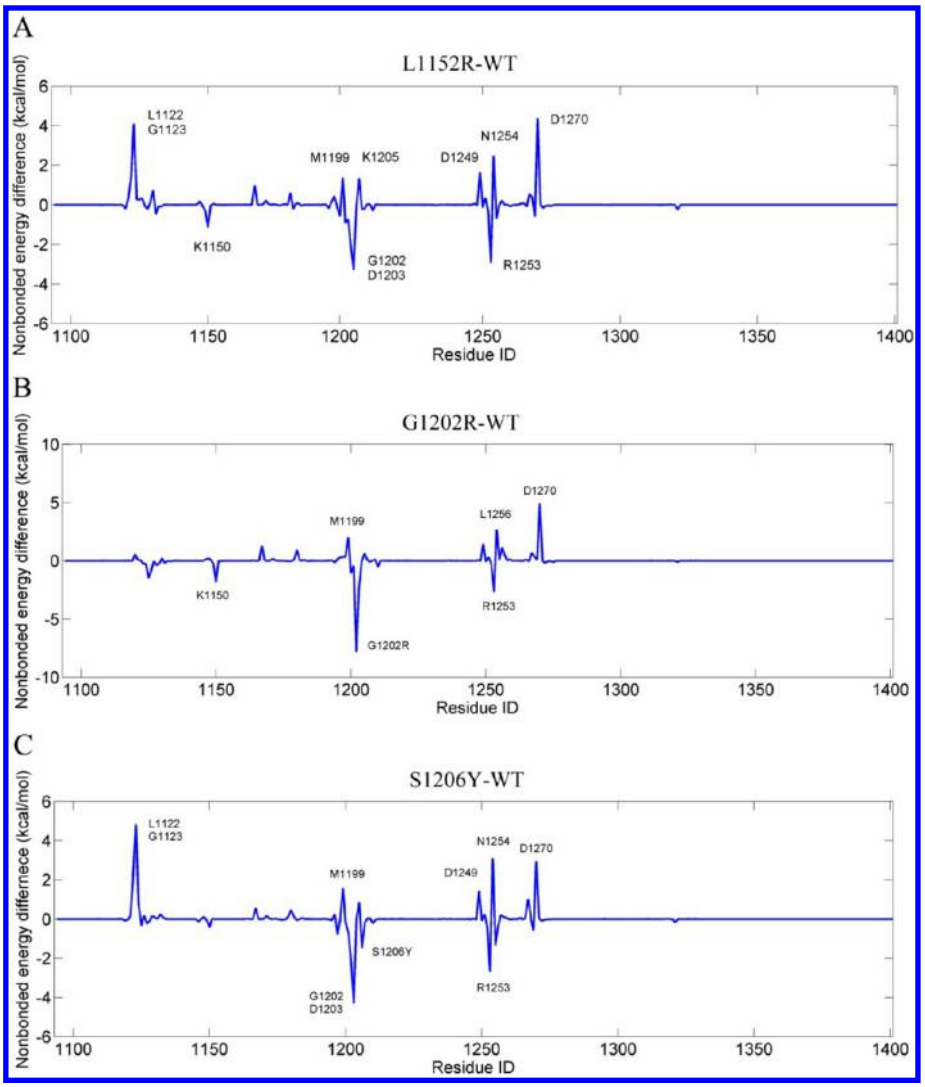

Figure 8. Distribution of the nonbonded interaction difference of the inhibitor−residue pairs between (A) WT and L1152R, (B) WT and G1202R (B), or (C) WT and S1206Y. The energy difference was calculated by $\Delta E = \Delta E_{MT} - \Delta E_{WT}$ where a positive ΔE indicates a weaker binding affinity in the mutated protein, and a negative ΔE indicates a stronger binding affinity.

the nonbonded energy was observed for G1202R (Table 2). The residue decomposition analysis shows that R1202 forms strong interactions (more than −7 kcal/mol) with crizotinib (Supporting Information Figure S5B and C). As shown in Figure 9B3, a strong H-bond is found between the guanidine of R1202 and N3 of crizotinib (yellow). Moreover, the bulky side chain of R1202 is favorable to strengthen the van der Waals interaction to crizotinib. Meanwhile, in G1202R, the H-bond between D1270 and the fluorine atom in crizotinib is weakened (3.8 versus 2.9 Å of the H-bond distance, Figure 9B2 and Supporting Information Figure S7A). The distribution of the differences of the nonbonded energies of the drug−residue pairs in S1206Y is

dx.doi.org/10.1021/ci400188q | J. Chem. Inf. Model. 2013, 53, 2376−2389

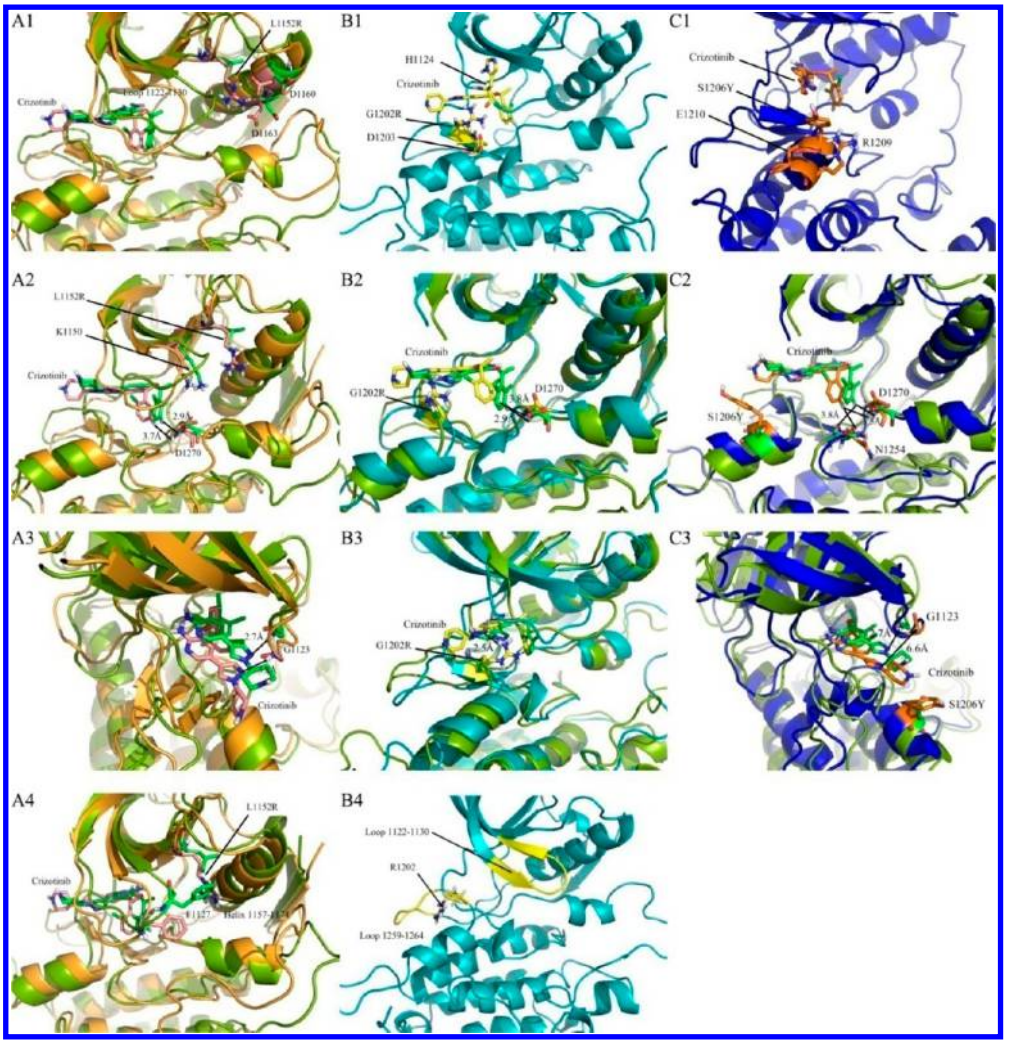

Figure 9. Superimposition of the average structures of the (A1−4) WT (dark green) and L1152R (orange), (B2 and B3) WT and G1202R (cyan), and (C2 and C3) WT and S1206Y (blue) ALK complexes. Crizotinib and several important residues are illustrated in stick model with the color green in WT, pink in L1152R, yellow in G1202R, and orange in S1206Y, respectively.

similar to that in L1152R (Figure 8C and A). The only difference is that there is a negative peak at the position S1206Y, suggesting that Y1206 can strengthen the nonbonded energy to crizotinib directly. In fact, the mutation S1206Y enhances the van der Waals energy to the drug binding as a result of the substitution of a small residue with a large one (Supporting Information Figure S6).

Figure 9C2 shows that, again, crizotinib locates more outside of the binding pocket and is close to the mutated residue Y1206 (orange). The mutation S1206Y drags the drug away from its original position in WT (green). Hence, the H-bond between D1270 and the fluorine in crizotinib is weakened and its distance increases from 2.9 to 3.5 Å (A time dependent evolution of the H-bond can be found in Supporting Information Figure S7A). Moreover, due to the rotation of the halogenated benzene fragment in crizotinib in S1206Y, the electrostatic repulsion between the oxygen atom in the backbone of N1254 and the fluorine in crizotinib increases, which leads to the decrease of the binding energy between N1254 and crizotinib in S1206Y (Figure 9C2). Similar to L1152R, the weakened mechanism of the H-bond between N3 in crizotinib (Figure 1) and the amide hydrogen of G1123 was also observed in S1206Y. However, the distance between the two atoms in S1206Y is bigger than that in L1152R (6.6 versus 3.8 Å). Thus, similar to L1152R, two important H-bonds were destroyed in S1206Y.

As shown in Table 2, if we do not consider the entropy term, the ranking result of the enthalpies for drug resistance is worse. The enthalpy for G1202R is even larger than that for WT (−41.34 kcal/mol versus −39.75 kcal/mol). Therefore, the conformational entropy plays an important role in the adjustment of the binding free energies for the ALK systems. As discussed above, the increase of the entropy term takes more than half of the decrease of the binding energies for L1152R and G1202R. As shown in Figure 10, the left column represents the entropy distribution for the unbound (or receptor) states of ALKs, and the right column shows those for the bound states of ALKs (or complex). The entropy was estimated from the covariance of the atomic fluctuations around crizotinib. The red regions on the bottom left of the complexes are all remarkably reduced compared with those in the corresponding unbound states of ALKs. However, the red areas at the top right of the complexes increase for WT (A) and S1206Y (D). There is no big difference for the complex of G1202R (C), and it decreases for the complex of L1152R (B). Further observation shows that the red areas at the bottom left and top right are located at the P-loop

dx.doi.org/10.1021/ci400188q | J. Chem. Inf. Model. 2013, 53, 2376−2389

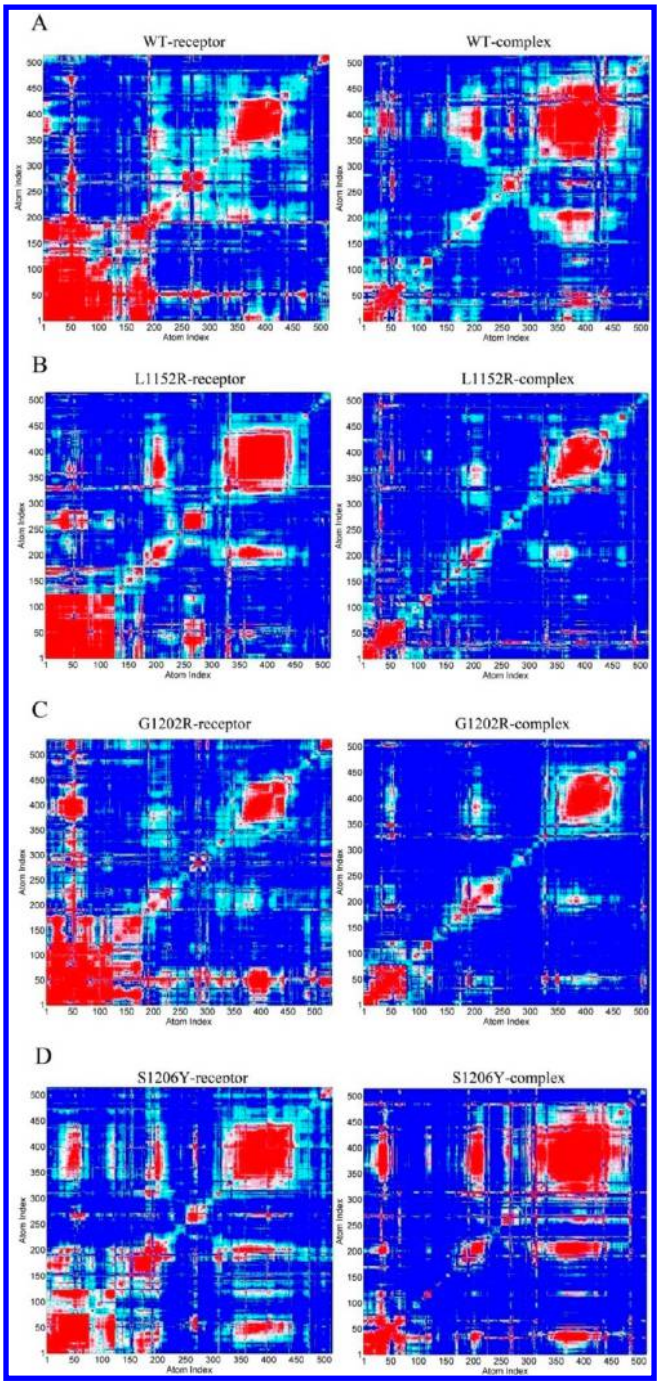

Figure 10. Covariance of the fluctuation of the heavy atoms located within 12 Å of crizotinib. The region colored in red indicates large amplitude of the atoms, which correlates with $|c_{ij}| > 0.5$, where c_{ij} is the covariance between the atoms i and j. While blue region stands for low amplitude atoms, which correlates with $|c_{ij}| < 0.2$. The left column represents the entropy distribution in the unbound states of ALKs, whereas the right column is the bound states of ALKs.

(loop 1122−1130) and loop 1259−1264 regions, respectively, in the ALK tyrosine kinase domain (yellow area in Figure 9B4).

Since the P-loop interacts with crizotinib directly, the binding state of the P-loop will lose conformational entropy substantially. The loop 1259−1264 locates outside of the binding pocket, and therefore, the change of the entropy depends on the binding state of crizotinib. The entropy of the loop 1259−1264 becomes larger in the bound state of ALK in WT. It may be explained by the fact that the binding position of crizotinib is more inside of the binding pocket compared with those in the mutated ALKs (Figure 9A2, B2, and C2) and the pyridine ring in crizotinib does not stabilize the loop 1259−1264, resulting in larger conformational entropy to the bound state of the WT ALK (Figure 10A).

Although crizotinib in S1206Y locates outside of the binding pocket compared with that in WT (Figure 8C2), its minimum region is wider (Figure 2D), which indicates that various conformations of crizotinib may be permitted in the binding pocket and thus the loop 1259−1264 may not be stabilized by crizotinib in S1206Y (Figure 10D). However, the pyridine ring of crizotinib in L1152R and G1202R indeed stabilizes the loop 1259−1264 because the top right red areas are remarkably reduced compared with those in WT and S1206R (Figure 10 right column). Because the loop 1259−1264 in the unbound state of G1202R is stabilized by the mutated residue R1202 (Figure 8B4), the red area at the top right of G1202R is much smaller than the other three areas at the same position in WT, L1152R, and S1206Y (Figure 10 left column). Thus, no decrease of the entropy in the loop 1259−1264 (red area at top right in Figure 10C) was observed between the bound and unbound states of G1202R. However, the increased flexibility of the loop 1259−1264 in the unbound state of L1152R results in the large decrease of the entropy at the top right region.

In consequence, L1152R leads to the largest change of the conformational entropy between its bound and unbound states, followed by G1202R, and then WT and S1206Y with a much smaller change of the entropy (−14.80 kcal/mol for WT and S1206Y, −20.25 kcal/mol for L1152R, and −19.01 kcal/mol for G1202R; see Table 1).

■ CONCLUSIONS

We successfully used the ABF simulations to calculate the binding free energies along the unbinding pathways of crizotinib from the binding sites of the WT and mutated ALKs. The comparison of the PMFs indicates that different reaction coordinates were employed by the WT and the three mutated ALKs. The *Z*-like route is used for WT, and the straight-like routes are for L1152R, G1202R, and S1206Y with different directions as shown in Figure 2.

The PMF depths (ΔW_{PMF}) derived from the ABF simulations are almost identical to the calculated standard binding free energies (ΔG°), which means no attention should be taken to distinguish the two energies based on the ABF simulations. A great difference was found between the results predicted by MM/GBSA based on the single and separated trajectory protocols, suggesting that the single MD trajectory protocol is more efficient and stable for the prediction of binding free energy for our systems. Importantly, all the protocols reproduced the right ranking results, which are in good agreement with the experimental data.

Residue decomposition shows that the decrease of the nonbonded energies for L1152R and S1206Y is primarily contributed from the loss of two important H-bonds due to the rearrangement of the drug. The drugs in the three mutated ALKs move a bit outside of the binding pocket compared with that in the WT ALK, which is consistent with the observations that the minimum position of crizotinib in the WT ALK is more inside than those in the three mutated ALKs as seen in Figure 2. However, the outward moving mechanisms are quite different: the moving out of K1150 repulsed by the positively charged mutated residue R1152 hinders the drug positioned at the original position in WT, the mutated residue R1202 stabilizes

dx.doi.org/10.1021/ci400188q | *J. Chem. Inf. Model.* 2013, 53, 2376−2389

crizotinib located outside of the original position by a strong H-bond, and the mutated residue Y1206 breaks the balance of crizotinib positioned at the inside position of the binding pocket and pulls it more outside of the pocket. (Figure 9A2, B2, and C2).

The entropy analysis shows that the P-loop (loop 1122−1130) and loop 1264−1259 play a vital role in the difference of the entropies between the bound and unbound states of ALKs. Because the P-loop interacts with crizotinib directly, all the bound states of ALKs show a decrease of the conformational entropy in the P-loop region compared with those in the corresponding unbound states of ALKs. However, the large difference of the entropies among the four systems is primarily contributed from loop 1264−1259. Due to the outside location of crizotinib in L1152R and G1202R, the pyridine ring of crizotinib stabilizes the loop 1264−1259, resulting in the loss of the conformational entropies in the bound states of L1152R and G1202R. However, the more inside location of crizotinib in WT and the wider minimum area of crizotinib in S1206Y possibly disturb the loop 1264−1259. Thus, it increases the conformational entropies in the bound states of ALKs in WT and S1206Y. Hence, the entropy changes of the crizotinib binding for L1152R and G1202R are much larger than those for WT and S1206Y.

In summary, for the first time, we clarify the drug resistance mechanisms of crizotinib conferred by three mutations in ALK by the combination of the ABF simulations and free energy calculations. It is feasible to develop small and nonchannel binding inhibitors to overcome the drug resistance caused by L1152R, G1202R, and S1206Y in ALK.

■ ASSOCIATED CONTENT

Supporting Information

Figure S1: Convergence of the potentials of mean force (PMFs). The PMFs gradually decrease with the simulation time increased, and when the simulation time was lengthened to 5−6 ns for each window, the PMFs are convergent. Figure S2: Root-mean-square deviations (RMSD, A−D) based on the backbone and root-mean-square fluctuations (RMSF, E) based on the heavy atoms of the WT (green) and mutated (orange, cyan, blue) ALKs and their corresponding crizotinib (pink). Figure S3: Superimposition of the PMFs along the *Z*-axis. The minimum energy position was used for overlapping the curves, and the highest of the PMF curve in WT (green) means the most energy will be produced when binding crizotinib to ALK. Figure S4: Distribution of the (A) nonbonded interaction difference, (B) electrostatic energy difference, and (C) van der Waals energy difference of the inhibitor−residue pairs between WT and L1152R. The energy difference was calculated by $\Delta E = \Delta E_{L1152R} - \Delta E_{WT}$ where a positive ΔE indicates a weaker binding affinity in the mutated protein, whereas a negative ΔE indicates a stronger binding affinity. Figure S5: Distribution of the (A) nonbonded interaction difference, (B) electrostatic energy difference, and (C) van der Waals energy difference of the inhibitor−residue pairs between WT and G1202R. The energy difference was calculated by $\Delta E = \Delta E_{G1202R} - \Delta E_{WT}$. Figure S6: Distribution of the (A) nonbonded interaction difference, (B) electrostatic energy difference, and (C) van der Waals energy difference of the inhibitor−residue pairs between WT and S1206Y. The energy difference was calculated by $\Delta E = \Delta E_{S1206Y} - \Delta E_{WT}$. Figure S7: H-bond distance between the F atom in crizotinib and NH atom in Asp1270 (A) and N3 atom in crizotinib and NH atom in Gly1123 (B). The two H-bonds in WT (green) are stronger than those in L1152R (orange), G1202R (cyan), and S1206Y (blue) in most simulation time. Table S1: Detailed information of binding free energy calculation using Henchman's method. Table S2: Binding free energies of crizotinib complexed with the WT and three mutated ALKs using the separated MD trajectory MM/GBSA approach (kcal/mol). This information is available free of charge via the Internet at http://pubs.acs.org. The following supplementary movies (Videos S1−S4) can be obtained from the authors upon request. Video S1: Unbinding process of crizotinib in WT. The light green region is the P-loop (loop 1122−1130) of ALK, and the yellow region represents the binding channel in the reaction coordinate that has been rotated to the screen. It can be found that when most of the molecule moves out of the binding pocket (expect the halogenated benzene fragment), crizotinib rotates to the P-loop side as there has greater space for it moving out without a large barrier (∼14 s), then the molecule turns and is absorbed at the binding channel (∼17 s), and finally it unbinds from the binding channel to the solvent (∼20 s). Video S2: Unbinding process of crizotinib in L1152R. The pink region is the P-loop (loop 1122−1130) of ALK, and the yellow region represents the binding channel in the reaction coordinate which has been rotated to the screen. It can be found that, when most of the molecule moves out of the binding pocket, it is hard for crizotinib to rotate to the P-loop side as the down moving of the P-loop, and thus the molecule can only be absorbed at the binding channel directly by overcoming a large barrier (∼12 s) and finally unbinds from the binding channel to the solvent (∼19 s). Video S3: Unbinding process of crizotinib in G1202R. The purple region is the mutated residue R1202, and the yellow region is the binding channel. It can be found that when the molecule moves out of the binding pocket, the first thing it should do is to push the mutated residue R1202 away, and the moved R1202 locates just above the binding channel (∼8 s), and thus, crizotinib can only go to the solvent without binding to the binding channel (∼15 s). Video S4: Unbinding process of crizotinib in S1206Y. The green region is the mutated residue Y1206, and the yellow region is the binding channel. It can be found that when the molecule moves out of the binding pocket, the fluctuation the side chain of Y1206 can constantly rotate and hinder the entrance of the binding channel, and thus, crizotinib can only go to the solvent without binding to the binding channel.

■ AUTHOR INFORMATION

Corresponding Authors

*E-mail: tingjunhou@hotmail.com or tingjunhou@zju.edu.cn. Phone: +86-512-65882039.

*E-mail: yyli@suda.edu.cn. Phone: +86-512-65882037.

Notes

The authors declare no competing financial interest.

■ ACKNOWLEDGMENTS

This study was supported by the National Science Foundation of China (21173156), the National Basic Research Program of China (973 program, 2012CB932600), the Priority Academic Program Development of Jiangsu Higher Education Institutions (PAPD), and the fund for Innovative Research Teams of Jiangsu Higher Education Institutions.

■ REFERENCES

(1) Crystal, A. S.; Shaw, A. T. New targets in advanced NSCLC: EML4-ALK. *Clin. Adv. Hematol. Oncol.* **2011**, *9*, 207−214.

(2) Kwak, E. L.; Bang, Y. J.; Camidge, D. R.; Shaw, A. T.; Solomon, B.; Maki, R. G.; Ou, S. H. I.; Dezube, B. J.; Jänne, P. A.; Costa, D. B.

Anaplastic lymphoma kinase inhibition in non-small-cell lung cancer. *N. Engl. J. Med.* **2010**, *363*, 1693−1703.
(3) Lovly, C. M.; Carbone, D. P. Lung cancer in 2010: One size does not fit all. *Nat. Rev. Clin. Oncol.* **2011**, *8*, 68−70.
(4) Mok, T. S. K. Personalized medicine in lung cancer: what we need to know. *Nat. Rev. Clin. Oncol.* **2011**, *8*, 661−668.
(5) Weickhardt, A. J.; Camidge, D. R. The therapeutic potential of anaplastic lymphoma kinase inhibitors in lung cancer: rationale and clinical evidence. *J. Clin. Invest.* **2011**, *1*, 1119−1126.
(6) Feliciano, P. Acquired resistance in lung cancer. *Nat. Genet.* **2012**, *44*, 241−241.
(7) Soda, M.; Choi, Y. L.; Enomoto, M.; Takada, S.; Yamashita, Y.; Ishikawa, S.; Fujiwara, S.; Watanabe, H.; Kurashina, K.; Hatanaka, H. Identification of the transforming EML4-ALK fusion gene in non-small-cell lung cancer. *Nature* **2007**, *448*, 561−566.
(8) Christensen, J. G.; Zou, H. Y.; Arango, M. E.; Li, Q.; Lee, J. H.; McDonnell, S. R.; Yamazaki, S.; Alton, G. R.; Mroczkowski, B.; Los, G. Cytoreductive antitumor activity of PF-2341066, a novel inhibitor of anaplastic lymphoma kinase and c-Met, in experimental models of anaplastic large-cell lymphoma. *Mol. Cancer Ther.* **2007**, *6*, 3314−3322.
(9) Gerber, D. E.; Minna, J. D. ALK inhibition for non-small cell lung cancer: from discovery to therapy in record time. *Cancer cell* **2010**, *18*, 548−551.
(10) Hallberg, B.; Palmer, R. H. Crizotinib–latest champion in the cancer wars? *N. Engl. J. Med.* **2010**, *363*, 1760−1762.
(11) Choi, Y. L.; Soda, M.; Yamashita, Y.; Ueno, T.; Takashima, J.; Nakajima, T.; Yatabe, Y.; Takeuchi, K.; Hamada, T.; Haruta, H. EML4-ALK mutations in lung cancer that confer resistance to ALK inhibitors. *N. Engl. J. Med.* **2010**, *363*, 1734−1739.
(12) Sasaki, T.; Okuda, K.; Zheng, W.; Butrynski, J.; Capelletti, M.; Wang, L.; Gray, N. S.; Wilner, K.; Christensen, J. G.; Demetri, G. The neuroblastoma-associated F1174L ALK mutation causes resistance to an ALK kinase inhibitor in ALK-translocated cancers. *Cancer Res.* **2010**, *70*, 10038−10043.
(13) Sasaki, T.; Koivunen, J.; Ogino, A.; Yanagita, M.; Nikiforow, S.; Zheng, W.; Lathan, C.; Marcoux, J. P.; Du, J.; Okuda, K. A novel ALK sondary mutation and EGFR signaling cause resistance to ALK kinase inhibitors. *Cancer Res.* **2011**, *71*, 6051−6060.
(14) Doebele, R. C.; Pilling, A. B.; Aisner, D. L.; Kutateladze, T. G.; Le, A. T.; Weickhardt, A. J.; Kondo, K. L.; Linderman, D. J.; Heasley, L. E.; Franklin, W. A. Mechanisms of Resistance to Crizotinib in Patients with ALK Gene Rearranged Non-Small Cell Lung Cancer. *Clin. Cancer Res.* **2012**, *18*, 1472−1482.
(15) Katayama, R.; Shaw, A. T.; Khan, T. M.; Mino-Kenudson, M.; Solomon, B. J.; Halmos, B.; Jessop, N. A.; Wain, J. C.; Yeo, A. T.; Benes, C. Mechanisms of acquired crizotinib resistance in ALK-rearranged lung cancers. *Sci. Transl. Med.* **2012**, *4*, 120ra117.
(16) Kobayashi, S.; Boggon, T. J.; Dayaram, T.; Jänne, P. A.; Kocher, O.; Meyerson, M.; Johnson, B. E.; Eck, M. J.; Tenen, D. G.; Halmos, B. EGFR mutation and resistance of non-small-cell lung cancer to gefitinib. *N. Engl. J. Med.* **2005**, *352*, 786−792.
(17) Katayama, R.; Khan, T. M.; Benes, C.; Lifshits, E.; Ebi, H.; Rivera, V. M.; Shakespeare, W. C.; Iafrate, A. J.; Engelman, J. A.; Shaw, A. T. Therapeutic strategies to overcome crizotinib resistance in non-small cell lung cancers harboring the fusion oncogene EML4-ALK. *Proc. Natl. Acad. Sci. U.S.A.* **2011**, *108*, 7535−7540.
(18) Lovly, C. M.; Pao, W. Escaping ALK inhibition: mechanisms of and strategies to overcome resistance. *Sci. Transl. Med.* **2012**, *4*, 120ps2.
(19) Bresler, S. C.; Wood, A. C.; Haglund, E. A.; Courtright, J.; Belcastro, L. T.; Plegaria, J. S.; Cole, K.; Toporovskaya, Y.; Zhao, H.; Carpenter, E. L. Differential inhibitor sensitivity of anaplastic lymphoma kinase variants found in neuroblastoma. *Sci. Transl. Med.* **2011**, *3*, 108ra114.
(20) Berry, T.; Luther, W.; Bhatnagar, N.; Jamin, Y.; Poon, E.; Sanda, T.; Pei, D.; Sharma, B.; Vetharoy, W. R.; Hallsworth, A. The ALK F1174L Mutation Potentiates the Oncogenic Activity of MYCN in Neuroblastoma. *Cancer cell* **2012**, *22*, 117−130.
(21) Sun, H. Y.; Ji, F. Q. A molecular dynamics investigation on the crizotinib resistance mechanism of C1156Y mutation in ALK. *Biochem. Biophys. Res. Commun.* **2012**, *423*, 319−324.
(22) Shen, L.; Ji, H. More on crizotinib. *N. Engl. J. Med.* **2011**, *364*, 777−778.
(23) Cui, J. J.; Tran-Dubé, M.; Shen, H.; Nambu, M.; Kung, P. P.; Pairish, M.; Jia, L.; Meng, J.; Funk, L.; Botrous, I. Structure Based Drug Design of Crizotinib (PF-02341066), a Potent and Selective Dual Inhibitor of Mesenchymal−Epithelial Transition Factor (c-MET) Kinase and Anaplastic Lymphoma Kinase (ALK). *J. Med. Chem.* **2011**, *54*, 6342−6363.
(24) Lee, C.; Jia, Y.; Li, N.; Sun, X.; Ng, K.; Ambing, E.; Gao, M.; Hua, S.; Chen, C.; Kim, S. Crystal structure of the ALK (anaplastic lymphoma kinase) catalytic domain. *Biochem. J.* **2010**, *430*, 425−437.
(25) Frisch, M.; Trucks, G.; Schlegel, H.; Scuseria, G.; Robb, M.; Cheeseman, J.; Montgomery Jr, J.; Vreven, T.; Kudin, K.; Burant, J. *Gaussian 03*; Gaussian, Inc.: Wallingford, CT, 2004.
(26) Bayly, C. I.; Cieplak, P.; Cornell, W.; Kollman, P. A. A well-behaved electrostatic potential based method using charge restraints for deriving atomic charges: the RESP model. *J. Phys. Chem.* **1993**, *97*, 10269−10280.
(27) Wang, J.; Wang, W.; Kollman, P. A.; Case, D. A. Automatic atom type and bond type perception in molecular mechanical calculations. *J. Mol. Graph. Model.* **2006**, *25*, 247−260.
(28) Wang, J.; Wolf, R. M.; Caldwell, J. W.; Kollman, P. A.; Case, D. A. Development and testing of a general amber force field. *J. Comput. Chem.* **2004**, *25*, 1157−1174.
(29) Hornak, V.; Abel, R.; Okur, A.; Strockbine, B.; Roitberg, A.; Simmerling, C. Comparison of multiple Amber force fields and development of improved protein backbone parameters. *Proteins: Struct., Funct., Bioinf.* **2006**, *65*, 712−725.
(30) Jorgensen, W. L.; Chandrasekhar, J.; Madura, J. D.; Impey, R. W.; Klein, M. L. Comparison of simple potential functions for simulating liquid water. *J. Chem. Phys.* **1983**, *79*, 926−935.
(31) Phillips, J. C.; Braun, R.; Wang, W.; Gumbart, J.; Tajkhorshid, E.; Villa, E.; Chipot, C.; Skeel, R. D.; Kale, L.; Schulten, K. Scalable molecular dynamics with NAMD. *J. Comput. Chem.* **2005**, *26*, 1781−1802.
(32) Darden, T.; York, D.; Pedersen, L. Particle mesh Ewald: An N log(N) method for Ewald sums in large systems. *J. Chem. Phys.* **1993**, *98*, 10089−10092.
(33) Ryckaert, J. P.; Ciccotti, G.; Berendsen, H. J. C. Numerical integration of the cartesian equations of motion of a system with constraints: molecular dynamics of n-alkanes. *J. Comput. Phys.* **1977**, *23*, 327−341.
(34) Feller, S. E.; Zhang, Y.; Pastor, R. W.; Brooks, B. R. Constant-pressure molecular-dynamics simulation-the Langevin piston method. *J. Chem. Phys.* **1995**, *103*, 4613−4621.
(35) Darve, E.; Rodríguez-Gómez, D.; Pohorille, A. Adaptive biasing force method for scalar and vector free energy calculations. *J. Chem. Phys.* **2008**, *128*, 144120−144132.
(36) Hénin, J.; Fiorin, G.; Chipot, C.; Klein, M. L. Exploring multidimensional free energy landscapes using time-dependent biases on collective variables. *J. Chem. Theory Comput.* **2009**, *6*, 35−47.
(37) Cai, W.; Sun, T.; Liu, P.; Chipot, C.; Shao, X. Inclusion Mechanism of Steroid Drugs into β-Cyclodextrins. Insights from Free Energy Calculations. *J. Phys. Chem. B* **2009**, *113*, 7836−7843.
(38) Dehez, F.; Pebay-Peyroula, E.; Chipot, C. Binding of ADP in the mitochondrial ADP/ATP carrier is driven by an electrostatic funnel. *J. Am. Chem. Soc.* **2008**, *130*, 12725−12733.
(39) Kekenes-Huskey, P. M.; Lindert, S.; McCammon, J. A. Molecular Basis of Calcium-Sensitizing and Desensitizing Mutations of the Human Cardiac Troponin C Regulatory Domain: A Multi-Scale Simulation Study. *PLoS Comput. Biol* **2012**, *8*, e1002777.
(40) Yang, L. J.; Zou, J.; Xie, H. Z.; Li, L. L.; Wei, Y. Q.; Yang, S. Y. Steered molecular dynamics simulations reveal the likelier dissociation pathway of imatinib from its targeting kinases c-Kit and Abl. *PloS One* **2009**, *4*, e8470.

(41) Petřek, M.; Otyepka, M.; Banáš, P.; Košinová, P.; Koča, J.; Damborský, J. CAVER: a new tool to explore routes from protein clefts, pockets and cavities. *BMC Bioinf.* **2006**, *7*, 316−325.
(42) Doudou, S.; Burton, N. A.; Henchman, R. H. Standard free energy of binding from a one-dimensional potential of mean force. *J. Chem. Theory. Comput.* **2009**, *5*, 909−918.
(43) Gumbart, J. C.; Roux, B. t.; Chipot, C. Standard Binding Free Energies from Computer Simulations: What Is the Best Strategy? *J. Chem. Theory Comput.* **2012**, *9*, 794−802.
(44) Woo, H.-J.; Roux, B. Calculation of absolute protein-ligand binding free energy from computer simulations. *Proc. Natl. Acad. Sci. U.S.A.* **2005**, *102*, 6825−6830.
(45) Deng, Y.; Roux, B. Computations of standard binding free energies with molecular dynamics simulations. *J. Phys. Chem. B* **2009**, *113*, 2234−2246.
(46) Li, L.; Li, Y.; Zhang, L.; Hou, T. Theoretical studies on the susceptibility of oseltamivir against variants of 2009 A/H1N1 influenza neuraminidase. *J. Chem. Inf. Model.* **2012**, *52*, 2715−2729.
(47) Hou, T.; Yu, R. Molecular dynamics and free energy studies on the wild-type and double mutant HIV-1 protease complexed with amprenavir and two amprenavir-related inhibitors: mechanism for binding and drug resistance. *J. Med. Chem.* **2007**, *50*, 1177−1188.
(48) Zhang, J.; Hou, T.; Wang, W.; Liu, J. S. Detecting and understanding combinatorial mutation patterns responsible for HIV drug resistance. *Proc. Natl. Acad. Sci. U.S.A.* **2010**, *107*, 1321−1326.
(49) Liu, H.; Yao, X.; Wang, C.; Han, J. In silico identification of the potential drug resistance sites over 2009 influenza A (H1N1) virus neuraminidase. *Mol. Pharm.* **2010**, *7*, 894−904.
(50) Beveridge, D. L.; DiCapua, F. Free energy via molecular simulation: applications to chemical and biomolecular systems. *Annu. Re V. Biophys. Biomol. Struct.* **1989**, *18*, 431−492.
(51) Gohlke, H.; Klebe, G. Approaches to the description and prediction of the binding affinity of small-molecule ligands to macromolecular receptors. *Angew. Chem., Int. Ed. Engl.* **2002**, *41*, 2644−2676.
(52) Jo, S.; Jiang, W.; Lee, H. S.; Roux, B.; Im, W. CHARMM-GUI Ligand Binder for Absolute Binding Free Energy Calculations and Its Application. *J. Chem. Inf. Model.* **2013**, *53*, 267−277.
(53) Jorgensen, W. L.; Thomas, L. L. Perspective on free-energy perturbation calculations for chemical equilibria. *J. Chem. Theory Comput.* **2008**, *4*, 869−876.
(54) Homeyer, N.; Gohlke, H. Free Energy Calculations by the Molecular Mechanics Poisson-Boltzmann Surface Area Method. *Mol. Inf.* **2012**, *31*, 114−122.
(55) Kollman, P. A.; Massova, I.; Reyes, C.; Kuhn, B.; Huo, S.; Chong, L.; Lee, M.; Lee, T.; Duan, Y.; Wang, W. Calculating structures and free energies of complex molecules: combining molecular mechanics and continuum models. *Acc. Chem. Res.* **2000**, *33*, 889−897.
(56) Wang, J. M.; Hou, T. J.; Xu, X. J. Recent advances in free energy calculations with a combination of molecular mechanics and continuum models. *Curr. Comput.-Aided Drug Des.* **2006**, *2*, 287−306.
(57) Onufriev, A.; Bashford, D.; Case, D. A. Exploring protein native states and large-scale conformational changes with a modified generalized born model. *Proteins: Struct., Funct., Bioinf.* **2004**, *55*, 383−394.
(58) Hou, T.; Wang, J.; Li, Y.; Wang, W. Assessing the performance of the MM/PBSA and MM/GBSA methods: I. The accuracy of binding free energy calculations based on molecular dynamics simulations. *J. Chem. Inf. Model.* **2011**, *51*, 69−82.
(59) Hou, T.; Wang, J.; Li, Y.; Wang, W. Assessing the performance of the molecular mechanics/Poisson Boltzmann surface area and molecular mechanics/generalized Born surface area methods. II. The accuracy of ranking poses generated from docking. *J. Comput. Chem.* **2011**, *32*, 866−877.
(60) Weiser, J.; Shenkin, P. S.; Still, W. C. Approximate atomic surfaces from linear combinations of pairwise overlaps (LCPO). *J. Comput. Chem.* **1999**, *20*, 217−230.
(61) Brooks, B.; Karplus, M. Harmonic dynamics of proteins: normal modes and fluctuations in bovine pancreatic trypsin inhibitor. *Proc. Natl. Acad. Sci. U.S.A.* **1983**, *80*, 6571−6575.
(62) Miller, B. R., III; McGee, T. D.; Swails, J. M.; Homeyer, N.; Gohlke, H.; Roitberg, A. E. MMPBSA.py: An Efficient Program for End-State Free Energy Calculations. *J. Chem. Theory Comput.* **2012**, *8*, 3314−3321.
(63) Lu, H.; Tonge, P. J. Drug-target residence time: critical information for lead optimization. *Curr. Opin. Chem. Biol.* **2010**, *14*, 467−474.
(64) Tummino, P. J.; Copeland, R. A. Residence Time of Receptor−Ligand Complexes and Its Effect on Biological Function. *Biochemistry* **2008**, *47*, 5481−5492.
(65) Masson, P.; Froment, M.; Bartels, C.; Lockridge, O. Importance of aspartate-70 in organophosphate inhibition, oxime re-activation and aging of human butyrylcholinesterase. *Biochem. J.* **1997**, *325*, 53−61.
(66) Amadei, A.; Linssen, A.; Berendsen, H. J. C. Essential dynamics of proteins. *Proteins: Struct., Funct., Bioinf.* **1993**, *17*, 412−425.
(67) Arcangeli, C.; Bizzarri, A. R.; Cannistraro, S. Concerted motions in copper plastocyanin and azurin: an essential dynamics study. *Biophys. Chem.* **2001**, *90*, 45−56.
(68) Chillemi, G.; Falconi, M.; Amadei, A.; Zimatore, G.; Desideri, A.; Di Nola, A. The essential dynamics of Cu, Zn superoxide dismutase: suggestion of intersubunit communication. *Biophys. J.* **1997**, *73*, 1007−1018.
(69) Schlitter, J. Estimation of absolute and relative entropies of macromolecules using the covariance matrix. *Chem. Phys. Lett.* **1993**, *215*, 617−621.
(70) Hou, T.; McLaughlin, W. A.; Wang, W. Evaluating the potency of HIV-1 protease drugs to combat resistance. *Proteins: Struct., Funct., Bioinf.* **2008**, *71*, 1163−1174.
(71) Hou, T.; Zhang, W.; Wang, J.; Wang, W. Predicting drug resistance of the HIV-1 protease using molecular interaction energy components. *Proteins: Struct., Funct., Bioinf.* **2009**, *74*, 837−846.
(72) Pan, D. B.; Sun, H. J.; Shen, Y. L.; Liu, H. X.; Yao, X. J. Exploring the molecular basis of dsRNA recognition by NS1 protein of influenza A virus using molecular dynamics simulation and free energy calculation. *Antiviral Res.* **2011**, *92*, 424−433.